

## Strong Ground Motion from the Michoacan, Mexico, Earthquake

J. G. ANDERSON, P. BODIN, J. N. BRUNE, J. PRINCE, S. K. SINGH,  
R. QUAAS, M. ONATE

---

The network of strong motion accelerographs in Mexico includes instruments that were installed, under an international cooperative research program, in sites selected for the high potential of a large earthquake. The 19 September 1985 earthquake (magnitude 8.1) occurred in a seismic gap where an earthquake was expected. As a result, there is an excellent description of the ground motions that caused the disaster.

---

ON 19 SEPTEMBER 1985, AN EARTHQUAKE OF MAGNITUDE 8.1 occurred with the epicenter near the Pacific coast of Mexico (1). Some damage occurred in the epicentral area, in Ciudad Guzman, and elsewhere outside of Mexico City. In Mexico City, 350 kilometers from the epicenter, the earthquake destroyed or badly damaged 300 (2) to 3,300 (3) buildings, and caused \$4 billion damage (3). The human toll was at least 8,000 dead or missing, 30,000 injured, and 50,000 homeless (3), out of a population of more than 18 million people. The earthquake occurred at 7:17 a.m. local time; had it occurred during business and school hours, the toll in lives could have been far greater because of the number of severely damaged school and office buildings. Damage in Mexico City was most concentrated in tall structures, with earthquake-resistant design features, which were subjected to shaking that was amplified by soft sediments below part of the city.

The earthquake came as no scientific surprise. It was caused by subduction of the Cocos Plate beneath Mexico (Fig. 1), the most active subduction thrust fault in the Western Hemisphere. Mexico has had 42 earthquakes with magnitude greater than 7 in this century associated with the subduction zone (4, 5), whereas California has had five associated with its correspondingly long San Andreas fault system. The 19 September earthquake occurred in the Michoacan seismic gap, which had been identified as a zone with high seismic potential by a variety of investigators (4, 6-13) with, however, speculation that the gap was permanently aseismic (4, 10, 12, 13).

The 19 September earthquake was documented by an array of strong motion accelerographs installed in the source region in expectation of this earthquake and what was considered an even more likely event in the nearby Guerrero seismic gap (Fig. 2).

---

J. G. Anderson, P. Bodin, and J. N. Brune are at the Institute of Geophysics and Planetary Physics, Scripps Institution of Oceanography, University of California at San Diego, La Jolla, CA 92093. J. Prince, S. K. Singh, R. Quaas, and M. Onate are at the Instituto de Ingenieria, Universidad Nacional Autónoma de México, Coyoacan 04510, C.U., México, D.F.

### International Cooperative Studies of Earthquake Ground Motion

The near-source recording of the 19 September Mexico earthquake is a success story in international cooperation. Before 1975, it was realized that international cooperative projects were crucial to increase the number of earthquake zones available for collecting data. Since earthquakes are relatively frequent in Mexico, the University of California, San Diego (UCSD), and the National Autonomous University of Mexico (UNAM) initiated in 1975 strong motion research in northern Baja California, Mexico, with National Science Foundation (NSF) support, resulting in important near-source recordings from two moderate earthquakes—the magnitude 6.6 Imperial Valley, California, earthquake of 15 October 1979, and the magnitude 6.1 Victoria, Baja California (Mexicali Valley), earthquake of 9 June 1980.

The importance of international cooperation was discussed at a workshop in 1978 in Honolulu, Hawaii (14). Several favorable array locations were identified, including the subduction zone of Oaxaca, Mexico, which, along with Taiwan, was given the highest probability (0.9) of recording accelerations greater than  $0.2g$  in 10 years (15). It seemed reasonable and important to extend the international program to the subduction zone along the west coast of Mexico. A large earthquake (magnitude 7.8) occurred in Oaxaca, Mexico, on 29 November 1978, making another large earthquake in that region less likely in the near future. After studying the seismicity pattern, we proposed to install an array in the Guerrero and Michoacan seismic gaps, northwest of Acapulco. The array of 29 instruments was being installed when the 19 September 1985 earthquake occurred. Twenty stations were in place and 16 high dynamic range digital records of ground motion were obtained (Fig. 2). The magnitude 7.5 aftershock, 36 hours later, was also recorded by the array.

### Seismic Prognosis for the Guerrero Gap

Repeat times of large earthquakes along a given portion of the Mexican subduction zone apparently average about 30 to 75 years (4, 12). However, successive large earthquakes can occur at shorter intervals in the same or nearby regions. Four large earthquakes occurred along the trench southeast of the 19 September event between 1899 and 1911; that region is now called the Guerrero seismic gap (Fig. 2), since it has not been the source of any large events since 1911.

In anticipation of large earthquakes recurring here, we concentrated the strong motion array southeast of the 19 September

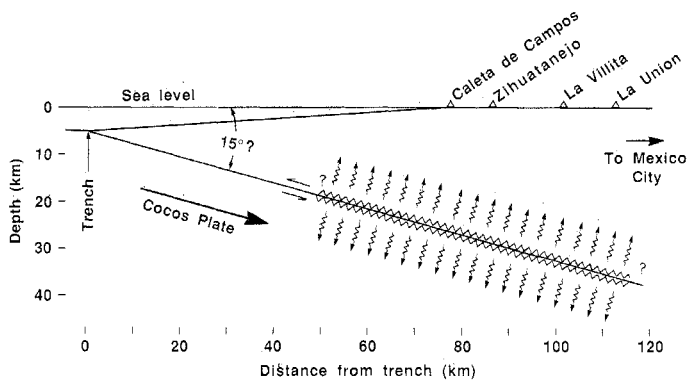


Fig. 1. Cross section of subduction of the Cocos Plate beneath the Mexican mainland. The illustrated extent of faulting corresponds to the aftershock zone in Fig. 3.

epicenter. Since the 19 September event did not fill the Guerrero gap, the likelihood of one or several large events there remains high, and recording the large earthquakes that will inevitably fill the gap remains an important short-term objective.

### Teleseismic Analysis

From free oscillations of the earth, the seismic moments were estimated to be  $10.3 \times 10^{27}$  dyne-cm and  $2.8 \times 10^{27}$  dyne-cm for the main shock and aftershock, respectively (16). The fault plane orientations for these solutions are estimated to strike  $105^\circ$  and dip  $18^\circ$ . The long-period *P*-waves recorded at Akureyri, Iceland (AKU), for the 19 and 21 September earthquakes are shown in Fig. 3. The

pulse from the 21 September event is simple; the 19 September event appears to be approximately the sum of two such sources with a time lag of about 26 seconds. The occurrence of the second event was in part responsible for the long source duration, but such long durations may be typical of earthquakes with magnitudes of at least 8 in this region.

In common with most Mexican earthquakes, aftershock activity was minimal from a teleseismic perspective: only 12 aftershocks with body wave magnitude ( $m_b$ ) of at least 3.7 were located in the 24 hours after the main shock; in the next 24 hours there were only four, including the aftershock with surface wave magnitude ( $M_S$ ) of 7.5; only one aftershock was recognized from teleseisms on 22 and 23 September.

Immediately after the earthquake, field crews went to the epicentral region to deploy sensitive instruments to record small aftershocks that would outline the rupture zone. Figure 2 shows preliminary determinations of the aftershock zones for the main event and large aftershock based on these data (17). The aftershock area of the 25 October 1981 earthquake ( $M_S = 7.3$ ) and the area to the south are relatively free of aftershocks (18).

### Strong Motion Recordings Near the Source

The locations of strong motion accelerographs on which the main shock on 19 September was recorded are shown in Fig. 2. These instruments are state-of-the-art digital recording accelerographs (19) and, like all accelerographs, are designed to operate remotely and unattended for months. When an earthquake occurs they sense the motion, turn on, record three components of ground motion including 2.5 seconds from pre-trigger memory, and turn off a few seconds after ground motion is below the trigger threshold. The

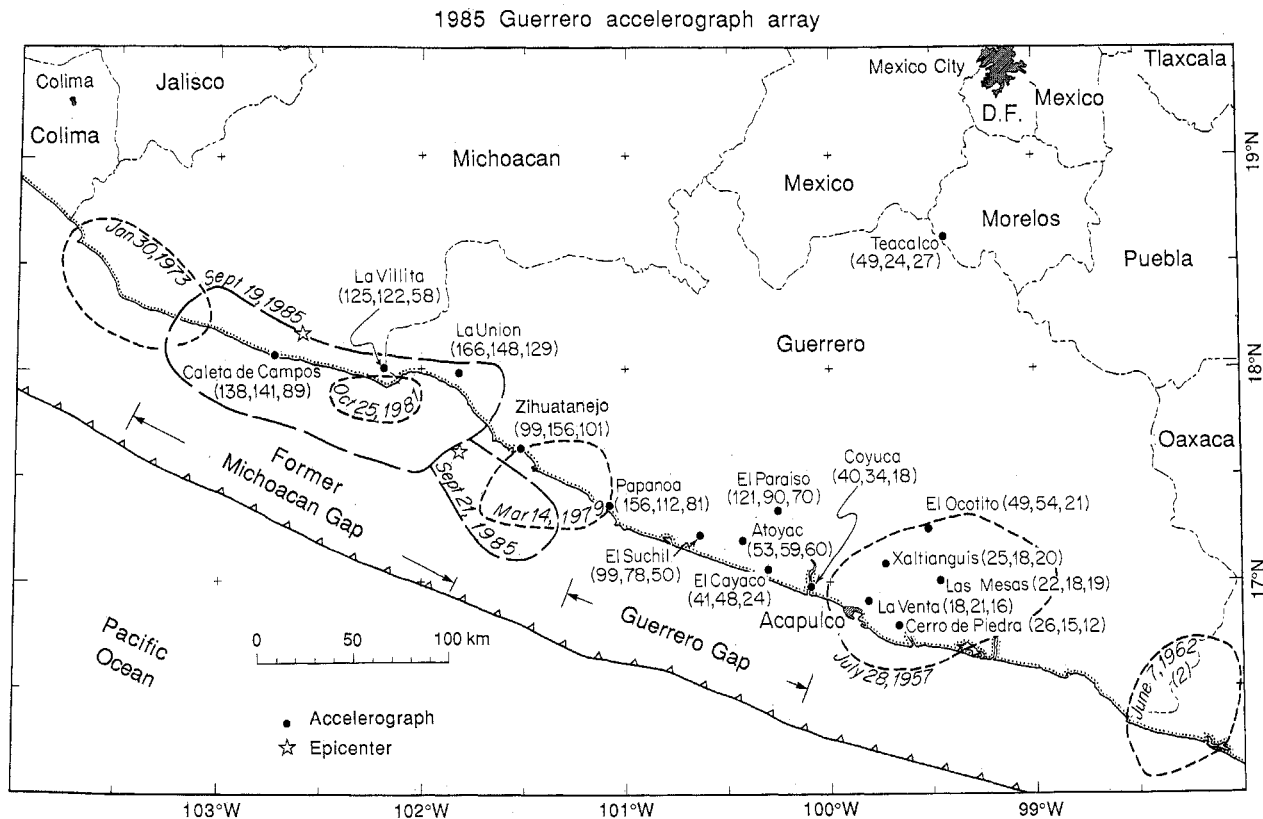


Fig. 2. Map of coastal Mexico, epicenters and aftershock zones of 1985 earthquakes in this region since 1951. Peak accelerations ( $\text{cm}/\text{sec}^2$ ) are given for each station for the north, east, and vertical components, respectively, in parentheses.

earthquakes in this region since 1951. Peak accelerations ( $\text{cm}/\text{sec}^2$ ) are given for each station for the north, east, and vertical components, respectively, in parentheses.



Fig. 3. Long-period vertical  $P$ -wave for the 19 and 21 September earthquakes recorded at station AKU (Akureyri, Iceland).

accelerograph stations were purposely located on hard crystalline basement rock to reduce near-surface effects. Thus motions in sediment-covered regions were probably considerably higher. All stations are equipped with clocks synchronized to Universal Time by Omega navigation signals.

Accelerographs at Caleta de Campos, La Villita, La Union, and possibly Zihuatanejo, were situated directly above the aftershock zone and inferred ruptured area (Fig. 2). Figure 4 shows the north-south component of acceleration from these four stations (20). Peak values (21) are listed on Fig. 2, about  $0.15g$  (150 gals) in the rupture region; durations of shaking in excess of  $0.1g$  were about 20 seconds. These accelerograms confirm that there were two "sub-events" in which energy release was relatively more intense, one near the epicenter and the second, starting about 24 seconds later, near La Union, separated by the aftershock zone of the October 1981 earthquake. At La Union and stations farther southeast, the energy from the two subevents arrived almost simultaneously. At La Villita and Caleta de Campos the two pulses were separated by about 20 seconds and 40 seconds, respectively. Caleta de Campos indicated a 3.2-second difference between the arrival times of the compressional and shear waves from the initiating event—that implies a hypocentral distance of less than 25 km. The gradual beginning suggests that the faulting was not immediately large.

Figures 5 and 6 show velocity and displacement at Caleta de Campos from the integrated accelerograms, and Fig. 7 shows north-south displacement at the stations directly above the fault. The integrations use a baseline correction proposed by Iwan *et al.* (22), and indicate a permanent displacement of the ground. At Caleta de

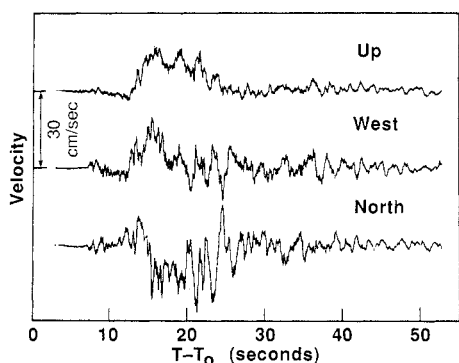


Fig. 5. Ground velocity at Caleta de Campos during the 19 September earthquake derived from accelerograms.

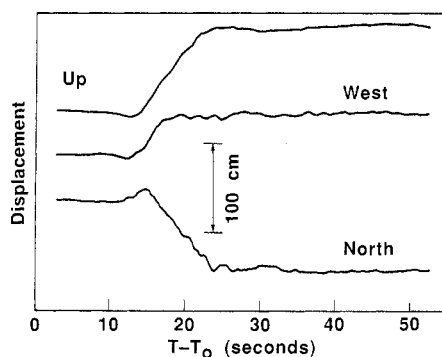


Fig. 6. Ground displacement at Caleta de Campos during the 19 September earthquake derived from accelerograms.

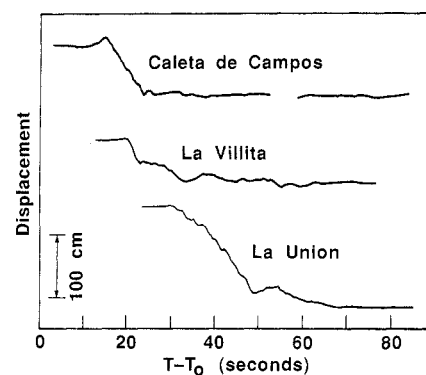


Fig. 7. North component of displacement at three stations above the aftershock zone.

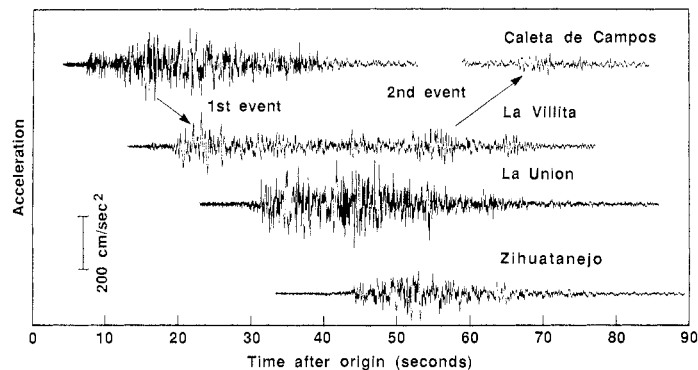


Fig. 4. North-south component of acceleration for stations above the aftershock zone. Vertical separation of traces is proportional to separation of the projection of stations onto the trench. Time,  $T_0$ , is the origin time of the earthquake (1). The clock correction at Caleta de Campos is uncertain.

Campos, displacements occurred over about a 10-second interval with ground velocity on each component averaging between 10 and 13 cm/sec, and the westward motion ceasing first. Such dynamic offsets during a major earthquake have never before been reliably recorded.

The directions of the offset (south, west, and up) are what one would expect from the plate tectonic model; the magnitudes are consistent with the average slip ( $\sim 230$  cm) obtained from the moment and fault area although we expected a smaller ratio of horizontal to vertical offsets. The vertical uplift at Caleta de Campos, 93 cm, is confirmed by the observation of about 1 m of permanent uplift along the coast (23). Caleta de Campos is located on a coastal terrace that might have formed seismically (10). This uplift generated a small tsunami (approximately 3 m locally at the coast).

On the basis of the data shown in Fig. 7 and the separations of the stations, the rupture front propagated with a velocity estimated at 3.8 km/sec from Caleta de Campos to La Villita, and 3.5 km/sec from La Villita to La Union. The major offset at Caleta de Campos begins about 8 seconds after the first  $S$ -wave arrived at the stations, suggesting some delay in the major faulting after the initiating event. The surface displacement took place over a time interval of about 10 seconds at Caleta de Campos and 20 seconds at La Union. At La Villita, integrations to displacement have higher relative uncertainties, but it appears that most displacement occurred in the initial 20 seconds, with some offset continuing until after the effects from faulting near La Union would have propagated back past the station. There are no indications of important precursory slip or post-rupture slip.

## Fourier Spectra

Fourier spectra from surface stations above a fault rupture of this size have not been observed before. Spectral ordinates (Fig. 8) increase with frequency from 0.1 to about 0.5 Hz, are relatively level to about 2 Hz, and generally decrease above 2 Hz, due to attenuation. At frequencies above 4 Hz, the spectrum from La Villita is smaller than those at the other two stations, consistent with less energetic rupture below La Villita and the attenuation of high frequencies which were radiated elsewhere on the fault. These spectra do not show a conspicuous peak at 0.5 Hz like spectra from the lake zone in Mexico City, although there is a relative maximum in the spectra from Caleta de Campos and La Union at that frequency, corresponding to visible oscillations on displacement traces (Fig. 7). From teleseisms the *P*-wave spectrum on 19 September resembles *P*-wave spectra from other recent large Mexican earthquakes; all are depleted from 0.1 to 1.0 Hz relative to a worldwide average (24). Near-field records from more earthquakes are needed to determine whether the source spectral amplitudes at 0.5 Hz are unusual, or typical, for this size of earthquake in Mexico. At frequencies higher than 0.1 Hz, the shape qualitatively resembles the far-field shape predicted by Gusev (25), although it differs in details.

For comparison, Fig. 8 shows the acceleration spectrum calculat-

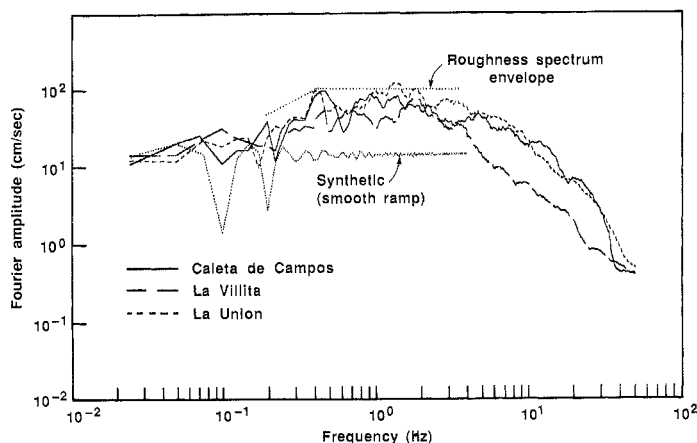


Fig. 8. Fourier amplitude spectra (smoothed) for the north-south components of acceleration above the aftershock zone.

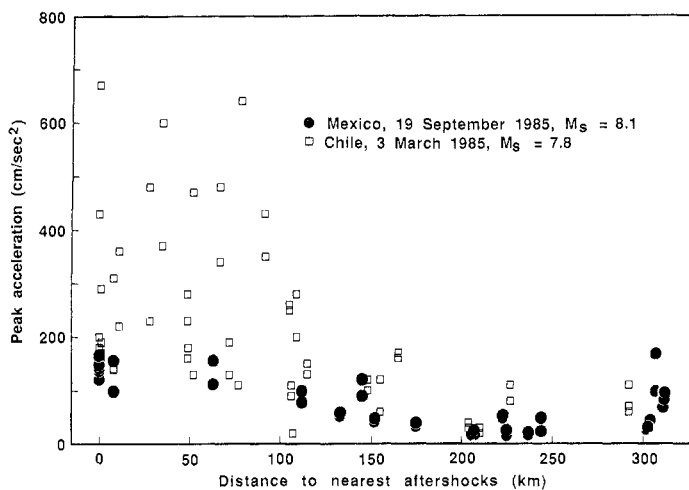


Fig. 9. Peaks of horizontal components of acceleration plotted against distance outside the boundary of the aftershock zone (Fig. 2).

ed for a synthetic seismogram consisting of a ramp displacement function, with displacement of 100 cm and a rise time of 10 seconds. Below 0.1 Hz, this generally agrees with the observed spectra, but from 0.3 to 3 Hz the observations are much larger, a consequence of fault-roughness causing radiation from relatively small areas on the fault surface that have stress drops perhaps exceeding 100 bars. A possible envelope for the roughness spectrum has a corner frequency of 0.5 Hz, corresponding to a source dimension with a 3- to 4-km radius (26) and, incidentally, to the resonant frequency of the sediments in Mexico City. From another viewpoint, relative to the high frequencies, which represent a higher stress drop over patches of the fault, the fault roughness can be thought of as introducing barriers, which cause partial stress drop averaged over the entire rupture (27), decreasing radiation at long periods.

## Energy and Stress Drop

The radiated seismic energy,  $E_S$ , is estimated by

$$E_S = \frac{1}{2} A \rho c \int v^2(t) dt \quad (1)$$

where  $A$  is the fault area,  $\rho$  and  $c$  are density and seismic wave velocity at the surface, and  $v(t)$  is the ground velocity. The integral is evaluated over the duration of the strong ground motion. Equation 1 assumes that the accelerograph, at which the surface velocity is amplified by a factor of 2 compared to the full space, is sufficiently near a uniformly radiating fault of area  $A$  that the limits of faulting do not affect the integral. Kinematic models and some modeling experiments suggest that Eq. 1 overestimates the energy radiated to the far field (28).

Energy estimates based on the strong motions observed at Caleta de Campos, La Villita, La Union, and Zihuatanejo indicate values for radiated energy of 1.2, 0.8, 1.3, and  $0.8 \times 10^{23}$  ergs, respectively. For  $c$  we used a shear-wave velocity of 2.9 km/sec and  $\rho$  of  $2.8 \text{ g cm}^{-3}$  as values appropriate for unweathered granite at the surface. The fault area, 50 by 170  $\text{km}^2$ , is derived from the aftershock zone on Fig. 2. About 50% of the energy on the north component at Caleta de Campos is associated with the smooth ramp, and 50% comes from the roughness; the roughness contributes less on other components.

The Gutenberg and Richter (29, 30) formula for energy gives, for  $M_S = 8.1$ ,  $E_S = 9 \times 10^{23}$  ergs. Our estimate is considerably smaller and suggests a relatively low dynamic stress drop in comparison with average earthquakes used to derive the formula.

We calculate three stress-change parameters for this earthquake. The static stress drop, 19 bars, is proportional to the average strain drop (approximation for a long, narrow dip-slip fault) (30). The apparent stress, obtained from radiated energy, is 6 bars or less since the energy may be overestimated. Apparent stress is expected to be 0.5 times the static stress (31). The effective dynamic stress, 6 to 12 bars (26, 32), relates particle velocity adjacent to a fault and the stresses that drive the faulting (32). These three estimates of stress drop are remarkably consistent, and indicate a relatively low stress drop and low energy release, which correlates with the relatively low values of peak ground acceleration recorded in the near field. None of the above estimates of stress drop can be used as a direct indication of absolute stress on the fault, since an unknown amount of energy goes into frictional heat generation. However, a profile of heat flow holes perpendicular to the coast (33) showed no evidence of any frictional heat generation along the fault. That study probably indicates an upper limit on frictional stresses of about 100 bars, consistent with estimates for the San Andreas fault (34). Therefore, the stress estimates from the seismic data, when combined with the observation of low heat flow, indicate low absolute stresses, proba-

bly less than 100 bars and perhaps as low as 20 bars. These low values of absolute stress have an important bearing on the physics of plate motion, since some plate tectonic models involve high absolute stresses at subduction zones.

## Attenuation with Distance

Figure 9 shows the peak horizontal accelerations recorded during the main shock, as a function of distance from the edge of the aftershock zone (Fig. 2). Peak values decrease with distance except for Mexico City and are considerably lower than expected based on extrapolation of the strong motion data gathered from shallower (5 to 15 km deep) earthquakes in California. For example, one empirical relation (35) extrapolates to  $1200 \text{ cm/sec}^2$  above the aftershock zone of a magnitude 8.0 earthquake, but predicts values less than half the values observed in Mexico at distances between 200 and 250 kilometers. However, the depth of faulting in Mexico on 19 September is greater than that for shallow strike-slip and thrust earthquakes in California (Fig. 1); it is not surprising that the peak accelerations at short distances from the epicenter in this earthquake are less than estimates based on California data, although we would not have expected them to be so much lower. Further study is needed to determine what factors, in addition to the differences in the depth of faulting and the low stress drop, might contribute to these lower levels of ground motion.

For comparison, Fig. 9 also shows peak accelerations recorded during the Chile earthquake ( $M_S = 7.8$ , 3 March 1985) (36), another subduction thrust earthquake with a geometry similar to the 19 September event. Peak accelerations for the Mexico data show much less scatter than the Chile data, and seem to be almost a lower bound. The depths to faulting in Chile and Mexico may be similar, but site conditions for the two sets of data are different. The Mexican stations at distances less than 300 km are generally on small piers on competent rock outcrops. The Chile site conditions are less uniform, generally in one- and two-story buildings and on a variety of volcanic or sedimentary rocks and alluvial deposits; these conditions result in resonances and amplification relative to basement rock, contributing to the scatter and higher values in peak accelerations. The scatter and the large amplitudes in Mexico City and at points beyond 300 km are obviously caused by site conditions. Other factors that might contribute to the higher accelerations in Chile than in Mexico are higher overall stress drop, failure of higher stress drop asperities, or triggered slip in the upper plate.

Higher peak accelerations have been observed in other Mexico subduction zone earthquakes. In the 21 September aftershock they reached  $245 \text{ cm/sec}^2$  at Papanao (21). A shallow magnitude 5 earthquake produced  $522 \text{ cm/sec}^2$  accelerations in Acapulco at an epicentral distance of about 35 km (37). The 19 March 1978 earthquake ( $M_S = 6.5$ ), located directly below Acapulco at a depth of 15 km, produced a peak acceleration of  $834 \text{ cm/sec}^2$  in Acapulco (38). An empirical relation for peak acceleration based on earlier Mexican data (38) predicts larger values at all distances except at Mexico City. Considering these results, and the Chile data, it would be premature to infer that the 19 September earthquake was typical of subduction thrust earthquakes, either in general or in Mexico.

## Strong Motion in Mexico City

The subsurface structure played an important role in determining the pattern and extent of damage in the Valley of Mexico. The near-surface geology of Mexico City, site of the former Lake Texcoco, may be classified into three general zones: the old lake bed, a hill

zone, and a transition zone between the two (Fig. 10) (2). The firmest near-surface materials are found in the hill zone, the southern edge of which is capped by 5 to 30 m of lava less than 2500 years old. The transition zone consists of river delta and shoreline deposits with interbedded intervals of clay. The lake bed zone is characterized by a deposit of very soft clay with high water content in the upper 30 to 40 meters.

Nearly all buildings that collapsed during the earthquakes of 19 and 21 September were located on the lake zone (Fig. 10). Ground motion was digitally recorded at four free-field sites on the hill and lake zones—UNAM, VIV (Viveros de Coyoacan), CDA (Central de Abastos), and SCT (Secretaria de Comunicaciones y Transportes). Other city sites were in buildings and may have been influenced by building response. The characteristics of the shaking at the various sites are related to the observed damage. Peak recorded accelerations are given in Fig. 10; Fig. 11 shows the most significant segment of the east-west components of acceleration. Not surprisingly, accelerograms on the hill zone (UNAM and VIV) show lower amplitudes and higher frequencies than accelerograms in the lake zone (CDA and SCT). The UNAM and VIV accelerograms are typical of prior observations in the hill zone, and the accelerograms from CDA and SCT are characteristic of prior observations in the lake zone (39, 40). Peak accelerations on 19 September are larger, possibly primarily a result of the larger magnitude.

The lake zone accelerograms have a long duration (5 minutes)

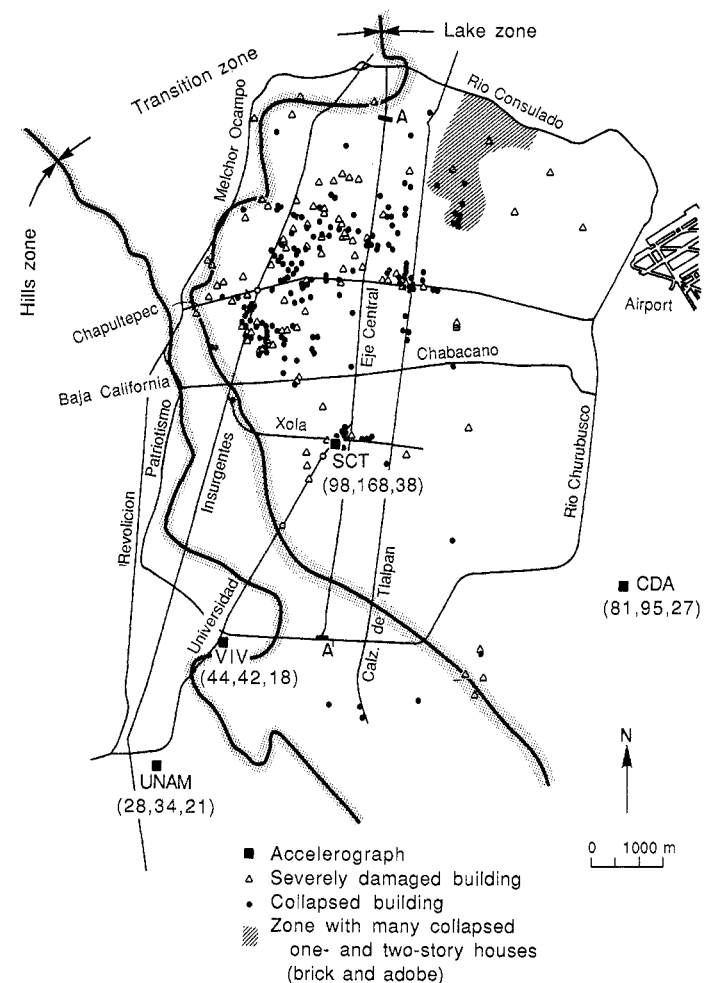


Fig. 10. Mexico City map showing free-field accelerograph stations, generalized soil classification, and sites of worst building damage from (2). Peak accelerations ( $\text{cm/sec}^2$ ) for the north, east, and vertical components, respectively, are given in parentheses by each station.

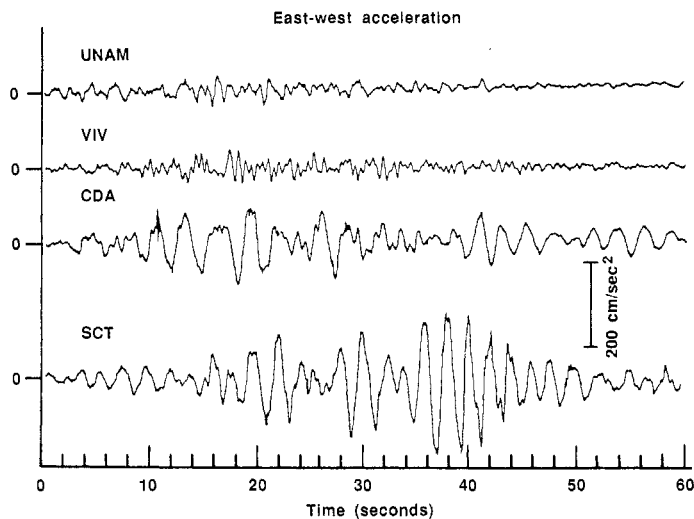


Fig. 11. Most significant 1-minute segments of the east-west acceleration recorded on the free-field accelerographs in Mexico City. Complete accelerograms are longer; 100 seconds of motion preceded the segment of the SCT record shown here. No time correlation exists among these traces.

with conspicuous long-period oscillations. Accelerograms from previous earthquakes at lake zone stations invariably are similar, with the low-frequency oscillations explained as resonant excitation of the shallow sedimentary structure (40, 41). Gravity anomalies indicate a buried, north-south ridge east of the heavily damaged area (42) which may also have modified the ground motion. Based on proximity and stronger similarities in the shallow geology, the SCT accelerogram is probably most representative of the excitation applied to building foundations in the heavily damaged area of the city. However, during the 14 March 1979 earthquake, an accelerograph in the basement of the Loteria Nacional building 4 km north of SCT showed accelerations 50 to 80% larger than the 1979 records at SCT. The Loteria record may have been modified by soil-structure interaction, but it reminds us that during the 19 September event some areas of the former lake bed may have experienced long-period shaking with amplitudes even larger than those recorded at SCT.

## Response Spectra

Structures in Mexico City are designed under a building code that requires earthquake-resistant features. As in the United States, this code provides for dynamic design of significant structures. The most common procedure is based on the concept of a design "response spectrum." A building with a given fundamental period of vibration is designed to resist a force proportional to the design "response spectrum" at that period. This may be compared with the actual "response spectrum," calculated from an observed accelerogram, which is proportional to the actual force to which the building was subjected (43).

Absolute acceleration response spectra (5% damping) for the four east-west accelerograms are compared in Fig. 12 with the corresponding design spectrum according to the latest revision (1977) of the Mexico City Building Code (44). Response spectra for UNAM and VIV do not exceed the design spectrum, correlating with the lack of damage in the hill zone. For CDA the spectrum is exceeded between from about 1.6 to 3.3 seconds by factors of up to 2.6, but there are no buildings higher than seven stories within a few kilometers of CDA, and the area was unscathed. At SCT the design spectrum is more significantly exceeded by the response spectrum; at

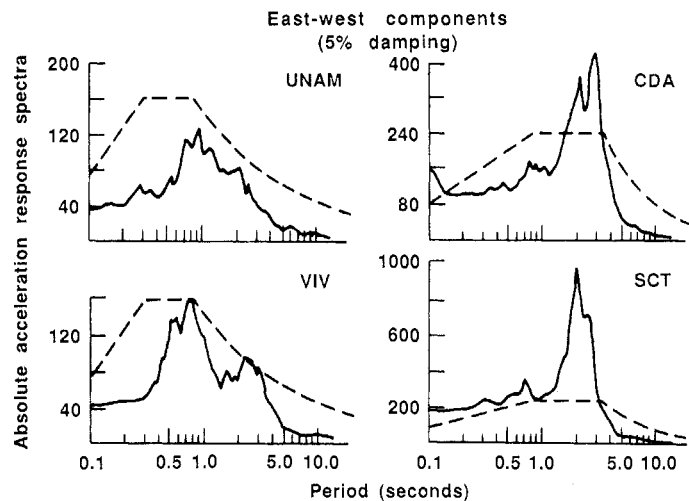


Fig. 12. Absolute acceleration response spectra (5% damping) for the accelerogram components in Fig. 11. Dashed lines are the applicable design spectra for the locations of each instrument.

2 seconds the factor is almost 4.2; this and the long time the spectral ordinate exceeded the design spectrum (over 25 seconds at a period of 2 seconds) were clearly excessive for many buildings. Within 300 m of SCT, eight buildings collapsed and several others were heavily damaged and had to be abandoned.

Within the primary damage zone, one estimate is that about 20% of the structures over six stories high suffered structural damage (2). For typical construction in Mexico the period in seconds of the fundamental mode of building vibration (fixed foundation) is usually about 0.1 times the number of stories. One effect of ductile behavior is to decrease the building stiffness and further increase the period during the shaking. Thus the high percentage of tall buildings that collapsed or were severely damaged correlates with the periods at which the design spectrum was exceeded by the earthquake motions.

## Conclusion

Because the epicentral regions of the tragic Mexican earthquakes were a well-instrumented seismic gap, a wealth of new observations on the mechanism of earthquake faulting and strong motion generation was obtained. More observations under similar conditions are needed before it can be known whether the observed low accelerations in the source region are anomalous or typical of such great earthquakes. Ground motion amplitudes had decreased with distance of propagation to harmless levels on rock sites near Mexico City, but selected frequencies were greatly amplified by the soft sediments of the Valley of Mexico. The worst damage occurred to structures that were near resonance with these amplified wave frequencies. Many of the questions left unanswered for this earthquake can be resolved if the Guerrero gap, which may rupture in the next decade or so, is properly instrumented.

## REFERENCES AND NOTES

1. "Preliminary determination of epicenters, No. 38-85" (National Earthquake Information Service, National Oceanic and Atmospheric Administration, Boulder, CO, 10 October 1985). The main shock epicenter is located at 18.182°N, 102.573°W, origin time 1300 hours 17 minutes 47.8 seconds Universal Time (UT),  $M_S = 8.1$ ,  $m_b = 7.0$ . From teleseisms, the primary aftershock is located at 17.823°N, 101.671°W, origin time 0100 hours 37 minutes 13.8 seconds UT,

- $M_s = 7.5$ ,  $m_b = 6.3$ . On the basis of local stations already in place, we have relocated the aftershock at 17.618°N, 101.815°W.
2. Instituto de Ingeniería de la Universidad Nacional Autónoma de México, *Informe Preliminar* (Mexico City, 1985).
  3. United Nations Economic Commission for Latin America and the Caribbean, *ECLAC, Report 85-10-1528* (1985).
  4. S. K. Singh, L. Astiz, J. Havskov, *Bull. Seismol. Soc. Am.* **71**, 827 (1981).
  5. S. K. Singh, M. Rodriguez, J. M. Espindola, *ibid.* **74**, 267 (1984).
  6. J. Kelleher, L. Sykes, J. Oliver, *J. Geophys. Res.* **78**, 2547 (1973).
  7. W. McCann, S. Nishenko, L. Sykes, J. Krause, *U.S. Geol. Surv. Open File Rep.* **78-943** (1978).
  8. A. Reyes, J. N. Brune, C. Lomnitz, *Bull. Seismol. Soc. Am.* **69**, 1819 (1979).
  9. R. P. Meyer *et al.*, *Geophys. Res. Lett.* **7**, 97 (1980).
  10. K. C. McNally and J. B. Minster, *J. Geophys. Res.* **86**, 4949 (1981).
  11. J. Havskov, S. K. Singh, E. Nava, T. Dominguez, M. Rodriguez, *Bull. Seismol. Soc. Am.* **73**, 449 (1983).
  12. L. Astiz and H. Kanamori, *Phys. Earth Planet. Int.* **34**, 24 (1984).
  13. L. V. LeFevre and K. C. McNally, *J. Geophys. Res.* **96**, 4495 (1985).
  14. W. D. Iwan, Ed., *Proceedings of the International Workshop on Strong Motion Instrument Arrays* (California Institute of Technology, Pasadena, 1978).
  15. University of California at Berkeley submitted a proposal in cooperation with investigators from Taiwan to install a strong motion array there. In 4 years it has recorded 35 earthquakes over a range of depths and distances and has been cost-effective in terms of quantity and quality of data acquired [B. A. Bolt and N. Abrahamson, *Bull. Seismol. Soc. Am.* **75**, 1247 (1985)]. Other arrays are planned in India, China, and Turkey.
  16. K. Priestley and G. Masters, *Geophys. Res. Lett.* **13**, 601 (1986).
  17. UNAM Seismology Group, *ibid.*, p. 573.
  18. There is a possibility of systematic offshore bias in our locations and in the locations of previous aftershock zones because of the complex structure of the downgoing slab (C. Stolte *et al.*, *ibid.*, p. 577).
  19. R. Quaa *et al.*, *Preliminary Report GAA-1B* (Instituto de Ingeniería, UNAM, Mexico City, 1985).
  20. At Caleta de Campos the instrument turned off before the intense energy from the southern source had arrived and started after a 6-second quiescence.
  21. J. G. Anderson *et al.*, *Preliminary Report GAA-LA* (Instituto de Ingeniería, UNAM, Mexico City, 1985).
  22. W. D. Iwan, M. Moser, C.-Y. Peng, *Bull. Seismol. Soc. Am.* **75**, 1225 (1985).
  23. P. Bodin and T. Klinger, *Science* **233**, 1071 (1986).
  24. H. Houston and H. Kanamori, *Geophys. Res. Lett.* **13**, 597 (1986).
  25. A. A. Gusev, *Geophys. J. R. Astron. Soc.* **74**, 787 (1983).
  26. A. Papageorgiou and K. Aki, *Bull. Seismol. Soc. Am.* **73**, 693 (1983).
  27. J. N. Brune, *J. Geophys. Res.* **75**, 4997 (1970).
  28. N. A. Haskell, *Bull. Seismol. Soc. Am.* **59**, 869 (1969); S. H. Hartzell and R. J. Archuleta, *J. Geophys. Res.* **84**, 3623 (1979); R. J. Archuleta and S. H. Hartzell, *Bull. Seismol. Soc. Am.* **71**, 939 (1981).
  29. B. Gutenberg and C. F. Richter give  $E_s$  (ergs) =  $10^{(11.8 + 1.5m)}$  [*Bull. Seismol. Soc. Am.* **46**, 105 (1956)].
  30. H. Kanamori and D. Anderson, *ibid.* **65**, 1073 (1975). The uncertainty in estimating static stress drop,  $(8/3\pi)\mu(D/w)$ , where  $\mu$  is shear modulus,  $D$  is average slip and  $w$  is fault width, is proportional to the uncertainty in estimating the width of the rupture zone based on aftershocks.
  31. Apparent stress is given by  $\mu E_s/M_0$ , where  $\mu$  is shear modulus,  $E_s$  is radiated energy, and  $M_0$  is moment [K. Aki, *Bull. Earthquake Res. Inst. Tokyo Univ.* **44**, 2388 (1966); M. Wyss and P. Molnar, *J. Geophys. Res.* **77**, 1433 (1972)].
  32. The effective dynamic stress is calculated from the equation of Brune (27),  $[(\mu/\beta)\bar{v}]$ , where  $\beta$  is shear velocity and  $\bar{v}$  is approximated by 0.5 times the average velocity at the surface during the ramp offset. Subsequent studies which remove simplifying assumptions of Brune find the rupture velocity replace the shear velocity  $\beta$ . The rupture velocity is unknown but is likely to be near the shear velocity. Foam rubber modeling of dynamic ruptures [J. N. Brune, *Bull. Seismol. Soc. Am.* **63**, 2105 (1973)] and calculations by H. Kanamori [*Phys. Earth Planet. Int.* **5**, 426 (1972)] indicate that the equations may give estimates of stress drop as much as a factor of 2 low.
  33. J. P. Ziaagos, D. D. Blackwell, F. Mooser, *J. Geophys. Res.* **90**, 5410 (1985).
  34. J. N. Brune, T. L. Henyey, R. F. Roy, *ibid.* **74**, 3821 (1969); A. H. Lachenbruch and J. H. Sass, *ibid.* **85**, 6185 (1980).
  35. W. B. Joyner and D. M. Boore, *Bull. Seismol. Soc. Am.* **71**, 2011 (1981).
  36. G. H. Saragoni, *Secc. Ing. Estruct. Univ. Chile* (1985); B. Bolt and N. A. Abrahamson, *Earthquake Eng. Res. Inst. Rep. 3 March 1985 Chile Earthquake* (1986).
  37. S. H. Hartzell, J. N. Brune, J. Prince, *Bull. Seismol. Soc. Am.* **68**, 1663 (1978).
  38. M. A. Bufaliza, thesis, Facultad de Ingeniería, Universidad Nacional Autónoma de México, Mexico City (1984).
  39. L. Alonso, J. M. Espinosa, I. Mora, D. Muria, J. Prince, *Inst. Ing. IPS-5A* (Universidad Nacional Autónoma de México, Mexico City, 20 March 1979).
  40. L. Zeevaert, *Bull. Seismol. Soc. Am.* **54**, 209 (1964).
  41. E. Rosenblueth, "Teoría del diseño sísmico sobre mantos blandos," *Ediciones ICA, B14* (Mexico, 1953); E. Faccioli and D. Resendiz, *Seismic Risk and Engineering Decisions*, C. Lomnitz and E. Rosenblueth, Eds. (Elsevier, New York, 1976), pp. 71-141.
  42. R. Alvarez, *Eos* **67**, 85 (1986).
  43. However, suitability of design criteria cannot be judged solely by the level of the design spectrum. The effects of ductility (ability of the structure to deform beyond the limits of elastic behavior without failure), differences between the true damping of the structure and assumed damping in the design spectrum, and durations of shaking are three other important effects that must be considered [G. W. Housner and P. C. Jennings, *Earthquake Design Criteria* (Earthquake Engineering Research Institute, Berkeley, CA, 1982)].
  44. In actual practice, the design spectra are reduced by a ductility factor ranging from 1 to 4. A large proportion of engineered structures in Mexico were undoubtedly designed with spectral ordinates one-half or less than those shown in Fig. 12.
  45. Supported by NSF grant CEE 82 19432. We thank D. Agnew and J. Berger for providing the very high quality IDA data used to determine the moment. D. Almora and P. Perez provided technical and field support, and E. Mena is responsible for computer processing of the data. We thank F. Vernon for his efforts in the aftershock studies. We also thank B. Bolt and N. Abrahamson for making their manuscript available to us in advance of publication and for sharing data on the 1985 Chile earthquake. J. E. Luco and E. Rosenblueth reviewed the manuscript.

